Available online at www.sciencedirect.com
ScienceDirect
Toxicology in Vitro 21 (2007) 492–501
Toxicology in Vitro
www.elsevier.com/locate/toxinvit

Estimating constants for metabolism of atrazine in freshly isolated rat hepatocytes by kinetic modeling

Tami S. McMullin [a,1], Melvin E. Andersen [b], John D. Tessari [a], Brian Cranmer [a], William H. Hanneman [a,*,1]

[a] Department of Environmental and Radiological Health Sciences, Campus Delivery, 132 Physiology Building, 1680, Colorado State University, Fort Collins, CO 80523, United States
[b] CIIT – Centers for Health Research, Research Triangle Park, NC 27709-2137, United States

Received 20 August 2006; accepted 21 October 2006
Available online 27 October 2006

Abstract

This study estimated the kinetic constants for oxidative metabolism of atrazine (ATRA) and its chlorotriazine (Cl-TRI) metabolites, 2-chloro-4-ethylamino-6-amino-1,3,5-triazine (ETHYL), 2-chloro-4-amino-6-isopropylamino-1,3,5-triazine (ISO), and diaminochlorotriazine (DACT), using freshly isolated rat hepatocytes. Hepatocytes were incubated with 1.74, 44, 98, and 266 μM ATRA. Disappearance of ATRA and formation of the Cl-TRI metabolites were quantified over 90 min. At all incubation concentrations, ATRA was preferentially metabolized to ETHYL, producing ETHYL concentrations approximately 6 times higher than those of ISO. DACT concentrations peaked at 44 μM ATRA and decreased with increasing incubation concentrations, indicating non-linear metabolic behavior of ATRA with respect to DACT formation. A series of kinetic models were developed from these data to describe the dose and time-dependent oxidative metabolism of ATRA and the Cl-TRI metabolites. An integrated model for all the chloro-triazines included multi-substrate competitive inhibition of metabolism to describe the non-linear behavior of DACT production in relation to ATRA while simultaneously simulating the time-course behavior of the Cl-TRIs at all four ATRA concentrations. The maximal metabolic rate (V_{max}) of ATRA metabolism and the Michaelis–Menten constant (K_M) for the reaction were 1.6 μM/min and 30 μM, respectively. V_{max} and K_M values for ETHYL and ISO metabolism to DACT were also estimated using this modeling approach.

Keywords: Kinetic modeling; Oxidative metabolism; Atrazine; Chlorotriazines; Competitive inhibition

1. Introduction

Atrazine (ATRA) is a chlorotriazine (Cl-TRI) herbicide that is widely used throughout the United States to control broadleaf and some grassy weeds (Gysin and Knuesli, 1960). ATRA undergoes extensive and rapid metabolism in the liver via cytochrome P450 mediated oxidation to chlorinated *N*-dealkylation products, 2-chloro-4-ethylamino-6-amino-1,3,5-triazine (ETHYL), 2-chloro-4-amino-6-isopropylamino-1,3,5-triazine (ISO), and diaminochlorotriazine (DACT) (Fig. 1). In rats, the substrate specificity toward ATRA is broad with several CYP family enzymes implicated in oxidation, including CYP2B2, CYP2C11, and CYP2D1 in male rats and CYP2B2, CYP2D1 and CYP2E1 in female rats (Hanioka et al., 1999b). In general CYP2E1 has a lower affinity for oxidation than other CYP family enzymes and is likely to be the predominant catalyst active at low concentrations (see Nakajima et al., 1990 and

Abbreviations: ATRA, atrazine; ISO, 2-chloro-4-amino-6-isopropylamino-1,3,5-triazine; ETHYL, 2-chloro-4-ethylamino-6-amino-1,3,5-triazine; DACT, diaminochlorotriazine; Cl-TRI, chlorotriazines; V_{max}, maximal velocity; K_M, Michaelis–Menten constant; PBPK, physiologically based pharmacokinetic; GSH, glutathione.

* Corresponding author. Tel.: +1 970 491 8635; fax: +1 970 491 7569.
E-mail address: hanneman@colostate.edu (W.H. Hanneman).
[1] Present address: The Dow Chemical Company, 1803 Building, Midland, MI 48674, United States.

0887-2333/$ - see front matter © 2006 Elsevier Ltd. All rights reserved.
doi:10.1016/j.tiv.2006.10.010

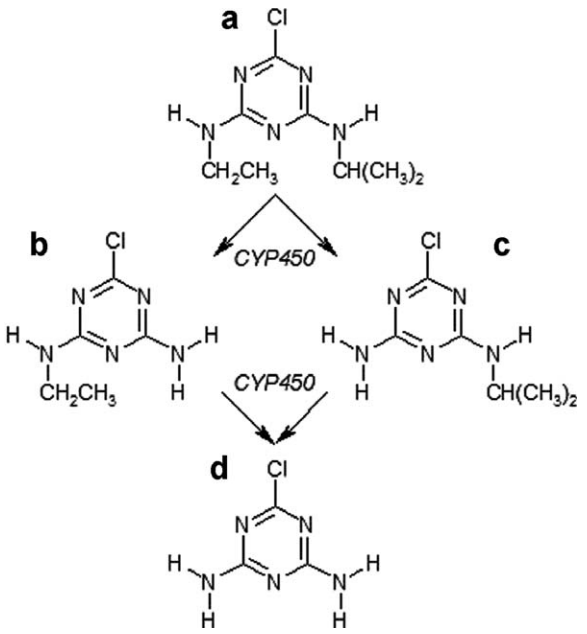

Fig. 1. Schematic of the P450 mediated oxidative metabolism of (a) atrazine (ATRA) to (b) 2-chloro-4-ethylamino-6-amino-1,3,5-triazine (ETHYL) and (c) 2-chloro-4-amino-6-isopropylamino-1,3,5-triazine(ISO), and subsequent metabolism to (d) diaminochlorotriazine (DACT).

ethanol-inducible metabolism). In addition to oxidative metabolism, the Cl-TRIs are metabolized to non-chlorinated compounds via glutathione *S*-transferase (GST) mediated GSH conjugation (Bakke et al., 1972; Dauterman and Mueke, 1973; Thede, 1987, 1988). High oral doses of ATRA or DACT cause neuroendocrine effects, including suppression of the steroid induced luteinizing hormone surge in adult, ovariectomized female rats (Cooper et al., 2000; McMullin et al., 2004). However, non-chlorinated metabolites of ATRA are toxicologically inactive (Eldridge et al., 2001). Thus, risk assessments for ATRA need to be based on net Cl-TRI doses to target tissues after ATRA exposures rather than administered dose.

Determination of internal dosimetry of Cl-TRIs requires an accurate description of oxidative metabolic clearance of these Cl-TRIs after exposure to ATRA. However, quantitative *in vivo* physiological descriptions of the kinetic disposition of ATRA and its chlorinated metabolites have been limited. A preliminary *in vivo* physiological pharmacokinetic model for ATRA was developed that used existing radioactivity and urinary data to estimate total Cl-TRIs in plasma, red blood cells and urine (McMullin et al., 2003). Due to the lack of time-course data on the individual compounds, this model was based on an aggregate estimate of total Cl-TRIs rather than studies that had tracked individual compounds separately. This earlier kinetic analysis was valuable in that it indicated the need to more thoroughly examine the time-course disposition of individual Cl-TRIs in order to provide information about the oxidative metabolic behavior of ATRA that leads to net tissue dosimetry of Cl-TRIs.

Subsequently, kinetic studies in rodents were conducted to evaluate the time-course of individual Cl-TRIs after oral gavage dosing with all four chlorotriazines (Brzezicki et al., 2003). Although these *in vivo* studies provided useful data for developing a more comprehensive physiologically based pharmacokinetic (PBPK) model to evaluate the disposition of individual Cl-TRIs, *in vitro* approaches are also needed to determine rates of oxidative metabolism that govern the *in vivo* kinetic behavior of these Cl-TRIs.

Oxidative metabolism of ATRA has been evaluated *in vitro* with kinetic studies using rat liver microsomes (Dauterman and Mueke, 1973; Hanioka et al., 1998, 1999b; Lang et al., 1996). Although data from microsomal studies are useful for determining P450 mediated product formation rates and comparing inter-species differences in metabolism, these data may not completely reflect the metabolic processes occurring *in vivo* (Billings et al., 1997) and be of limited use for extrapolation to describe *in vivo* metabolism. In contrast, several kinetic studies using freshly isolated rat hepatocytes have provided metabolic parameters that correlate well with *in vivo* metabolism (Chenery et al., 1991; Sirica and Pitot, 1979; Thurman and Kauffman, 1979). These type of data have been successfully integrated into PBPK models to describe *in vivo* metabolism of chemicals such as benzene (Cole et al., 2001) and furan (Kedderis et al., 1993) and pharmaceutical agents (Andersson et al., 2001).

The goal of this study was to determine *in vitro* kinetic parameters for oxidative metabolism of ATRA to the chlorinated metabolites from time-course studies using incubations with freshly isolated rat hepatocytes. A series of kinetic models were used to describe the dose and time-dependent kinetic behavior of ATRA and the two mondealkyated Cl-TRI metabolites. The kinetic parameters derived from these models serve as initial estimates for describing the metabolic clearance pathways occurring *in vivo* that lead to total Cl-TRI tissue dose.

2. Materials and methods

2.1. In vitro time-course study

2.1.1. Chemicals

ATRA (97.1% purity), ETHYL (97.1% purity), ISO (97.1% purity) and DACT (96.8% purity) were generously provided by Syngenta Corporation (Greensboro, NC). Earles' balanced salt solution without $CaCl_2$ and $MgCl_2$ (EBSS) was obtained from Sigma Chemical Co. (St. Louis, MO). Hepatocyte Wash Buffer was from GIBCO. Dimethylsulfoxide (DMSO), distilled diethyl ether (EE), Optima grade acetone, *n*-hexane, iodomethane (stabilized 99%), and tetra-butyl-ammonium hydroxide (TBAOH) were from Fisher Chemical Company (Houston, TX). Cyanazine (CYA; 99% purity) was from Sigma Chemical Company (St. Louis, MO).

Standards of ATRA, ETHYL, ISO, and CYA (all at 4.6 mM) were prepared in acetone. DACT was prepared in

DMSO at 6.87 mM. Stock solutions were diluted to working concentrations of 4.6 and 46.3 and 463 μM in acetone.

2.1.2. Hepatocyte preparations

Female Sprague–Dawley rats (200–300 g) were obtained from Charles River laboratories and held at Colorado State University Laboratory Animal Research facility. All procedures were approved by Colorado State University Animal Care and Use Committee. The isolation of hepatocytes followed the procedure by Seglen (1976) with some modifications. Upon anesthetizing the animal and catheterizing the portal vein, the liver was perfused with Buffer A (500 ml EBSS, 7.5 mM HEPES, 100nM Dexamethasone, 0.75 mM EGTA) and 5 ml Penicillin–Streptomycin (Pen–Strep) for 5 min and subsequently perfused with Buffer B (500 ml EBSS, 10mM HEPES, 2.5 mM $CaCl_2$, 100 nM Dexamethasone, 5 ml Pen–Strep, and 0.04% Collagenase) for 5 min. The liver was removed and washed with Hepatocyte Wash Buffer with gentle stirring for 1.5 min. Only perfused lobes were used for subsequent hepatocyte isolation.

Cells were filtered to remove tissue debris and placed in 50 ml conical vials. Hepatocyte Wash buffer was added to bring the volume to 50 ml. The cellular suspension was centrifuged at 500 rpm (IEC HN-SII centrifuge) for 2 min. After removal of the supernatant, the pellet was re-suspended in Hepatocyte Wash Buffer and centrifuged 2 additional times (500 rpm). This process ensures <10% contamination by non-hepatocyte cells (Berry and Friend, 1969). The final pellet was reconstituted to 50 ml with Hepatocyte Wash Buffer and gently mixed. Isolations yielding ⩾80% viability, as determined by the trypan blue exclusion assay, were used for metabolism studies.

2.1.3. Experimental design

Hepatocytes (2×10^6 cells/ml) were added to flasks containing 10 ml EBSS fortified with 2% bovine serum albumin (BSA). The flasks were continuously shaken at 37 °C under 5%CO_2 in air. After a 15 min. acclimation period, ATRA was added directly to the flasks at concentrations of 1.74, 44.0, 98.0, and 266.0 μM in 0.01% DMSO. A control group consisting of frozen, untreated hepatocytes and hepatocytes spiked with an internal standard mixture of ATRA, ETHYL, ISO, DACT and CYA (surrogate standard) were analyzed within each set of unknown time-course samples. Aliquots (100 μl) of the media were collected at 0, 30, 60, and 90 min to monitor the disappearance of ATRA and simultaneous appearance of chlorinated metabolites. Samples were stored at −20 °C until analysis. At all concentrations, cell viability at 90 min was determined to be >90%. Four separate time course experiments were run for 1.74 and 44 μM ATRA. Two separate experiments were run for 98 and 266 μM ATRA. Results are plotted as the mean ± SD of all studies at each concentration.

2.1.4. Analytical methods

Frozen control and time-course samples were analyzed following published methods (Brzezicki et al., 2003). Each sample was thawed and extracted over EE (3×2 ml) with gentle mixing at room temperature for 10 min and followed by centrifugation (2 min) to separate the EE phase. Extracted samples were placed in glass culture tubes (6 ml) and evaporated to complete dryness under a steady stream of nitrogen. Acetone (100 μl) in azeotrope residual water was added to the sample and evaporated under nitrogen for 20 min.

Derivatization of all analytes in the samples and standards was performed by adding DMSO (100 μl), tetrabutyl ammonium hydroxide (5 μl), *n*-hexane (500 μl), and methyl iodide (30 μl). Tubes were capped and rotated at room temperature for 30 min. After rotation, deionized water (1 ml) and *n*-hexane (2 ml) were added to all tubes and shaken for 2 min. The methylated analytes were extracted into the *n*-hexane phase (3×). Extracts were dried to <100 μl under nitrogen. Sample volumes were brought to 100 μl with *n*-hexane.

Derivatized analytes were analyzed by GC–MS (Hewlett Packard 5890 Gas Chromatograph equipped with a Model 5972 mass-selective detector). Concentrations were quantified using calibration curves. Analyte recoveries were ±20% of mean recovery values obtained during daily method validation.

2.2. Kinetic modeling

2.2.1. Model structures

A series of kinetic models were developed in order to analyze the hepatocyte kinetic data while accounting for changes in time-course concentrations of substrate and product. In these models, the oxidative metabolism of ATRA, ETHYL and ISO is presumed to be catalyzed by the same cytochrome P450 enzyme. ATRA is metabolized via saturable oxidative metabolism in a process that leads to both ETHYL and ISO. Appearance of ETHYL and ISO in the incubation system is determined by the rate of metabolism of ATRA and the fraction metabolized to each mono-dealkylated metabolite (frac). Formation of DACT occurs from oxidative metabolism of the mono-dealkylated metabolites to DACT.

The data at the higher concentrations of ATRA (98 μM and 266 μM) indicated dose-dependent non-linear formation of DACT. To account for reduced conversion to DACT at higher incubation concentrations, the final model included competitive inhibition between substrates, as noted in the following equations:

$$\mathrm{dMETatra}/\mathrm{d}t = (V_{\max}\mathrm{atra} * \mathrm{Catra})/(\mathrm{Catra} + \mathrm{Katra} * (1 + \mathrm{Ciso}/\mathrm{Kiso} + \mathrm{Cethyl}/\mathrm{Kethyl} + \mathrm{Cdact}/\mathrm{Kdact}))$$

$$\mathrm{dMETiso}/\mathrm{d}t = (V_{\max}\mathrm{iso} * \mathrm{Ciso})/(\mathrm{Ciso} + \mathrm{Kiso} * (1 + \mathrm{Cethyl}/\mathrm{Kethyl} + \mathrm{Catra}/\mathrm{Katra} + \mathrm{Cdact}/\mathrm{Kdact}))$$

$$\mathrm{dMETethyl}/\mathrm{d}t = (V_{\max}\mathrm{ethyl} * \mathrm{Cethyl})/(\mathrm{Cethyl} + \mathrm{Kethyl} * (1 + \mathrm{Catra}/\mathrm{Katra} + \mathrm{Ciso}/\mathrm{Kiso} + \mathrm{Cdact}/\mathrm{Kdact}))$$

In these equations, *C* terms designate concentration of the chloro-triazine in the test tube. The terms, dMETatra/d*t*,

dMETiso/dt and dMETethyl/dt, are the rates of metabolism of ATRA, ISO and ETHYL, respectively. V_{max}atra is the maximal velocity of the enzyme metabolizing ATRA to ETHYL and ISO. V_{max}ethyl and V_{max}iso are the maximal velocities of the enzymes converting the mono-dealkylated metabolites to DACT. Katra, Kiso and Kethyl are the binding affinities (i.e., the effective Michaelis–Menten constants for binding) for ATRA, ISO and ETHYL, respectively. These metabolism terms were then included in a set on mass balance differential equations that track each chloro-triazine and DACT over time (see below). The initial value conditions for the 4 compounds, set in the equations here as "init" followed by the name of the compound were equal to either the initial ATRA concentration in the incubations or zero for the other three Cl-TRIs. The equations were solved numerically over time using a Rosenbrock algorithm for the integration.

dCatra/dt = rate loss by oxidative metabolism to ISO and ETHYL
initCatra = Catra0
dCiso/dt = rate of formation by ATRA dealkylation − rate of loss by oxidation to DACT
initCiso = 0.0
dCethyl/dt = rate of formation by ATRA dealkylation − rate of loss by oxidation to DACT
initCethyl = 0.0
dCdact/dt = rate of formation by ETHYL oxidation + rate of formation by ISO oxidation
init Cdact = 0.0

Initially, first-order loss rates were also included to account for non-oxidative clearance such as glutathione conjugation and/or production of non-chlorinated products. The addition of the first-order pathway did not improve the ability of our kinetic models to describe these *in vitro* results, indicating that, at least in this *in vitro* setting, clearance of these Cl-TRIs is predominantly via oxidative dealkylation. Because of this observation we limited our equations to describing oxidation.

Model code was written using Berkeley–Madonna modeling software (version 8.0.1 for Windows; (Robert I. Macey and George F. Oster, University of California, Berkeley, California)). Computer code for our Cl-TRI models can be obtained by contacting the first author, Dr. Tami McMullin. The curve-fit routine in Berkeley–Madonna, which minimizes the root mean square deviation between the data points and the model output, was used to optimize the various model parameters against the time-course data with the 4 compounds at 4 concentrations.

3. Results

3.1. Experimental observations

At all incubation concentrations, heteroatom dealkylation of ATRA by CYP450 preferentially attacked the isopropyl group, resulting in ETHYL concentrations up to 6 times higher than ISO. Depletion of ATRA from the solution and production of the mono-dealkylated metabolites ETHYL and ISO were time and dose-dependent over the entire monitoring period (Table 1). Initial attempts to fit this entire body of time course data with a single model produced unrealistic parameter values for several of the Michaelis constants (Table 2). It was apparent that a more systematic approach to analyzing these time course curves would be necessary. To do this, a series of three kinetic models were developed to determine *in vitro* kinetic constants for oxidative metabolism of ATRA to its chlorinated metabolites in a system where substrate and product concentrations were dose and time-dependent.

Table 1
Time-course data of atrazine (ATRA), 2-chloro-4-amino-6-isopropylamino-1,3,5-triazine (ISO), 2-chloro-4-ethylamino-6-amino-1,3,5-triazine (ETHYL) and diaminochlorotriazine (DACT) after incubating hepatocytes with (a) 1.7 μM ATRA, (b) 44 μM ATRA, (c) 98 μM ATRA and (d) 266 μM ATRA[a]

Time (min)	ATRA	ISO	ETHYL	DACT
(a) 1.7 μM				
0	1.74 ± 0.12	0 ± 0.12	0 ± 0.16	0 ± 0.12
30	1.18 ± 0.05	0.13 ± 0.03	1.36 ± 0.05	0.86 ± 0.24
60	0.37 ± 0.12	0.37 ± 0.12	1.5 ± 0.12	1.40 ± 0.15
90	0.11 ± 0.22	0.39 ± 0.01	1.49 ± 0.13	1.65 ± 0.13
(b) 44 μM				
0	44.1 ± 5.0	0 ± 1.5	0.23 ± 3.0	0 ± 0.05
30	15.1 ± 1.3	1.5 ± 0.51	13.0 ± 0.25	1.3 ± 0.5
60	4.3 ± 1.4	3.1 ± 2.2	22.2 ± 1.6	3.1 ± 0.3
90	0.31 ± 2.5	4.2 ± 3.5	26.6 ± 4.2	3.3 ± 0.6
(c) 98 μM				
0	98.1 ± 5.0	0.28 ± 4.0	0.2 ± 7.0	0.14 ± 0.05
30	78.3 ± 4.0	5.2 ± 6.7	6.5 ± 2.5	0.84 ± 0.12
60	29.8 ± 7.5	12.9 ± 8.0	32.5 ± 5.5	1.8 ± 0.68
90	12.6 ± 10.0	14.5 ± 6.2	37.7 ± 2.5	3.2 ± 0.24
(d) 266 μM				
0	265 ± 10	0.14 ± 6.5	0.76 ± 7.0	0.14 ± 0.12
30	230 ± 2.3	3.7 ± 10.2	9.2 ± 4.9	0.28 ± 0.22
60	170 ± 14.5	10 ± 10.3	63.5 ± 16.5	0.84 ± 0.4
90	118 ± 6.8	16.7 ± 4.7	89.4 ± 3.9	2.2 ± 0.15

[a] Data are expressed as mean ± SD.

3.2. Model structures and applications

Instead of using an unconstrained fitting procedure for estimating the kinetic constants, a sequential parameterization process was pursued. This approach utilized three individual kinetic models (Models I through III) that were developed based on the dose-dependent kinetic behavior of the compounds. The first model described the kinetic behavior of ATRA metabolism at the lowest concentration (1.7 μM) where oxidative metabolism is below enzyme saturation, leading to a single first-order rate constant for metabolism, Katra = V_{max}atra/$K_M$atra, that regulates loss of ATRA from the suspensions. This study was conducted near the limit of detection for DACT, leading to challenges

Table 2
Model estimated parameters used in the final kinetic model that accounts for multi-substrate competitive metabolic inhibition

Parameter		Global parameterization	Sequential parameterization
V_{max}atra (μmol/200 × 10^6 cells/min)	Maximum metabolic rate of ATRA to ETHYL and ISO	0.88	1.6
V_{max}ethyl (μmol/200 × 10^6 cells/min)	Maximum metabolic rate of ETHYL to DACT	0.196	0.07
V_{max}iso (μmol/200 × 10^6 cells/min)	Maximum metabolic rate of ISO to DACT	0.0006	0.12
$K_M$atra (μM)	Michaelis–Menten constant for ATRA	15.4	30
$K_M$ethyl (μM)	Michaelis–Menten constant for ETHYL	4.9	13
$K_M$iso (μM)	Michaelis–Menten constant for ISO	2.8	13
Frac	Fraction of ATRA metabolized to ISO	0.14	0.15

in accurate determination of the concentration of this metabolite. However, loss rates for ATRA and appearance of the two mono-dealkylated metabolites were still adequately captured by this data set and the modeling analysis (Fig. 3).

After establishing a first-order metabolism rate constant in Model I, Model II was developed to estimate Michaelis–Menten constants for ATRA oxidation under conditions with higher substrate concentration. The data from the 44 μM ATRA incubation resulted in peak DACT concentrations (Figs. 2 and 4), suggesting that metabolism of ATRA was approaching the maximal velocity of the enzyme (V_{max}atra). Therefore, metabolism of ATRA to the mono-dealkylated metabolites at this concentration was limited by V_{max}atra. Using saturable Michaelis–Menten kinetics, Model II provided initial estimates of both V_{max}atra and $K_M$atra, that themselves constrained to give the ratio for V_{max}atra to $K_M$atra from Model I. V_{max}atra was estimated by fitting while holding all other parameters constant. After fitting to estimate V_{max}atra, $K_M$atra was estimated using the equation V_{max}atra/$K_M$atra = Katra (the first-order transition rate determined in Model I). Because oxidative metabolism of the mono-dealkylated metabolites to DACT is likely catalyzed by P450 enzymes similar to those that catalyze ATRA oxidation to the mono-dealkylated metabolites, initial values of $K_M$ethyl and $K_M$iso were set to equal $K_M$atra and then V_{max}ethyl and V_{max}iso were estimated by fitting the same data set. In this way, Models I and II together served as an initial constraint on the V_{max} and K_M values utilized to estimate model parameters from all the data sets.

Model III was used to determine final kinetic parameter values that described the entire data set while incorporating dose-dependent metabolic behavior of the compounds. The data at the higher concentrations (98 μM and 266 μM) indicated that DACT production was complexly related to the initial ATRA concentration peaking at 44 μM and falling at higher incubation concentrations (Figs. 2, 5 and 6). This dose-response curve for DACT at 90 min was used as the primary dataset for parameter estimation and then the values obtained from this fit were assessed for their ability to simulate all other data sets. The V_{max} and K_M values for ETHYL and ISO were fixed at the values determined in Model II. The dose-response for DACT at 90 min was visually fit by varying V_{max}atra and $K_M$atra until a fit to the entire dose-response curve was obtained. Berkeley Madonna does not have the tools to do the fit across multiple concentrations as necessary in Fig. 2 using a least squares approach.

In these models, ATRA metabolism to the mono-dealkylated metabolites was described by a saturable process with a V_{max} of 1.6 μmol/l/min and K_M of 30 μM. The proportion of ATRA metabolized to ISO and ETHYL was 15% and 85%, respectively. Clearance of the mono-dealkylated metabolites to DACT via oxidative metabolism, estimated by V_{max}/K_m, was approximately 10-fold lower than

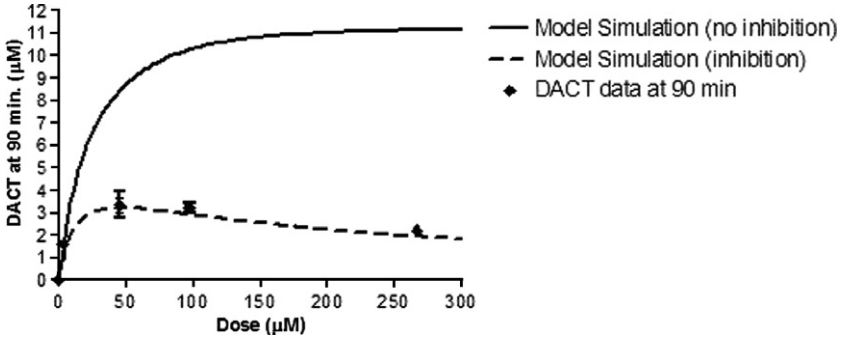

Fig. 2. DACT dose-response at 90 min comparing model simulations with and without competitive metabolic inhibition terms. The non-linear behavior of DACT formation could only be simulated with a model that included competitive inhibition of oxidative metabolism by all Cl-TRIs. Lines represent model simulations. Points represent data means ± SD. The model simulation here was derived from the best fit parameters to Model III used to simulate DACT production for all 4 incubation concentrations.

the clearance of ATRA to the mono-dealkylated metabolites (Table 2).

Unlike the mono-dealkylated metabolites, peak DACT production occurred at 44 μM and decreased with increasing substrate concentrations. This non-linear characteristic of ATRA metabolism with respect to DACT indicated that inhibition was likely occurring in the incubation system and therefore, was also examined in the kinetic analysis. Although a model description of the oxidative metabolism of ATRA that included Michaelis–Menten kinetics with no substrate inhibition simulated the datasets at the lowest concentrations, it greatly overestimated the higher concentrations DACT where non-linearity of DACT formation was observed (Fig. 2). Inclusion of inhibition of metabolism more accurately described the time-course concentrations of ATRA, ETHYL and ISO while simultaneously estimating the non-linear behavior of DACT over all 4 concentrations (Figs. 3–6). This model provided final estimates of the *in vitro* metabolic parameters for ATRA metabolism to the Cl-TRIs (Table 2). Although the final model accounted for competition by all Cl-TRIs for the same metabolizing enzyme, ATRA and the mono-dealkylated metabolites mainly contributed to the overall inhibition since DACT concentrations were minimal relative to the other Cl-TRIs in all these incubations.

4. Discussion

In this study, freshly isolated rat hepatocytes were incubated with concentrations of ATRA that resulted in dose-dependent kinetic behaviors of the Cl-TRIs over 90 min. The preferential metabolism of ATRA to ETHYL over ISO observed in the current study using rat hepatocytes is consistent with previous *in vivo* and *in vitro* time-course studies. The clearance of ATRA due to oxidative metabolism to ETHYL was 10-fold greater than oxidative metabolic clearance to ISO in microsomal incubations (Hanioka et al., 1999a,b). Similarly, an oral gavage dose of 150 mg ATRA/kg b.w. produced peak ETHYL concentrations that were approximately 3× greater than ISO (Brzezicki et al., 2003). This metabolic disposition of ATRA is most likely due to preferential attack by the P450 oxidative enzyme on the –CH group adjacent to the nitrogen in the ISO side-chain of ATRA rather than the methylene group adjacent to the nitrogen in the ETHYL side chain.

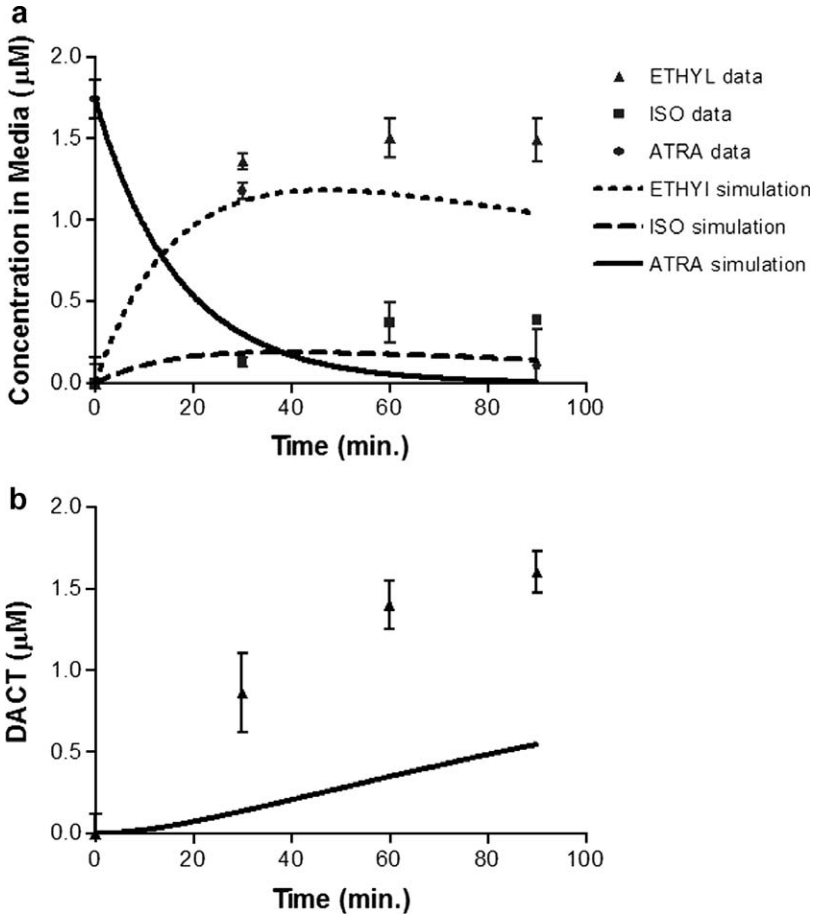

Fig. 3. Experimental data and competitive inhibition model simulations of (a) ATRA, ETHYL, ISO and (b) DACT after 1.74 μM ATRA treatment. Lines represent model simulations. Points represent data means ± SD. The best fits were developed using Model III after sequential model building efforts to constrain the parameter space searched by the fitting algorithm.

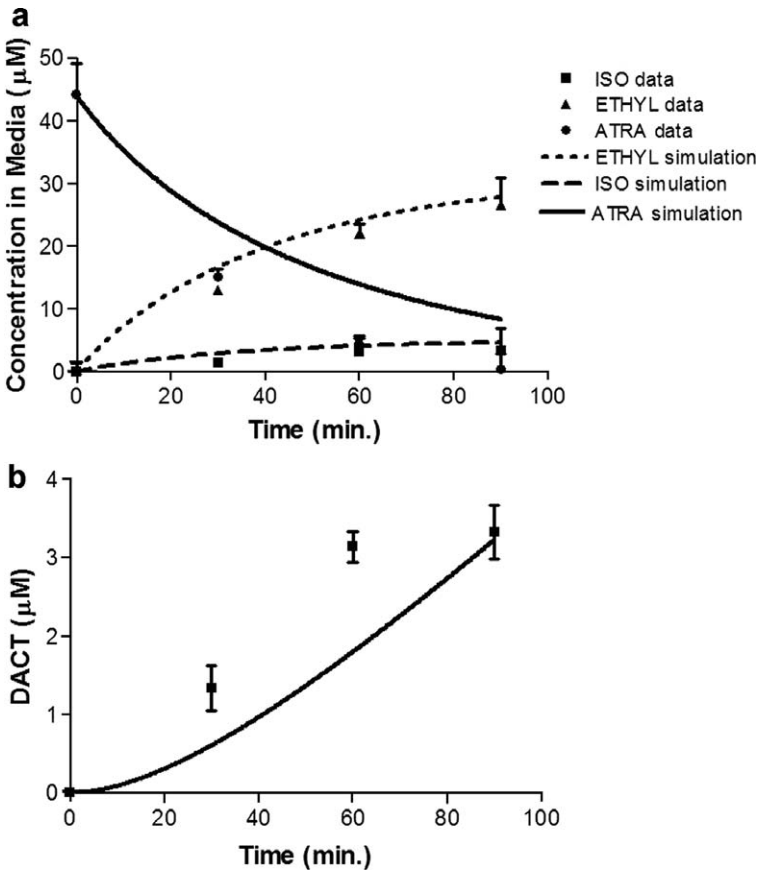

Fig. 4. Experimental data and competitive inhibition model simulations of (a) ATRA, ETHYL, ISO and (b) DACT after 44 μM ATRA treatment. Lines represent model simulations. Points represent data means ± SD. The best fits were developed using Model III after sequential model building efforts to constrain the parameter space searched by the fitting algorithm.

4.1. Determining kinetic constants for oxidative metabolism of ATRA

A quantitative description of the oxidative metabolism of ATRA is necessary for predicting net tissue dose to Cl-TRI from exposure to ATRA in the environment. To determine the Michaelis–Menten kinetic parameters for saturable oxidative metabolism of ATRA to its chlorinated metabolites, a sequential kinetic modeling approach was developed to analyze data generated in freshly isolated rat hepatocytes. A first attempt to parameterization utilized a global approach to fit all parameters simultaneously with a single model. Without a strategy for parameter estimation by curve fitting, the constants obtained from the global fit gave extremely low Michaelis–Menten values that were biologically unrealistic and inconsistent with previously published results (Hanioka et al., 1999a,b) (Table 2). Instead of using an unconstrained fitting procedure for estimating the kinetic constants, a sequential parameterization process was applied based on the observed dose-dependent kinetic behavior of the Cl-TRIs.

This step-wise kinetic analysis provided kinetic constants for the oxidative metabolism of ATRA that are consistent with the values reported in previous time-course studies using microsomes. Converting the *in vitro* values to common *in vivo* units assuming 128×10^6 heptocytes/g liver (Seglen, 1976), V_{max} value for ATRA to the mono-dealyated metabolites is 0.2 mmol/h/kg. Using the model estimated fraction of ATRA metabolism to ISO of 0.15, V_{max} for ATRA to ISO and ETHYL determined in our hepatocyte incubation system are 0.03 mmol/h/kg and 0.17 mmol/h/kg, respectively. Hanioka et al. (1999a,b) report similar V_{max} values for ATRA metabolism to ISO of 0.01–0.012 mmol/h/kg and ATRA metabolism to ETHYL of 0.12–0.15 mmol/h/kg. Moreover, the K_M value for ATRA metabolism to ETHYL and ISO ($K_M$atra) determined in this *in vitro* system was 30 μM. This value agrees well with the estimates of Hanioka et al. (1999a,b) (50 μM) while also providing adequate fits to the time-course data and simulating the dose-response curve of DACT at 90 min.

In vitro and *in vivo* studies using each mono-dealkylated metabolite as a substrate indicate that oxidative metabolism of ISO results in significantly more DACT than metabolism of ETHYL (Dauterman and Mueke, 1973; Brzezicki et al., 2003). The kinetic analysis performed in this study similarly predicted a larger contribution of DACT formation from ISO metabolism, as estimated by V_{max}/K_M. Although these time-course results indicate some level of DACT production after ATRA incubation, DACT

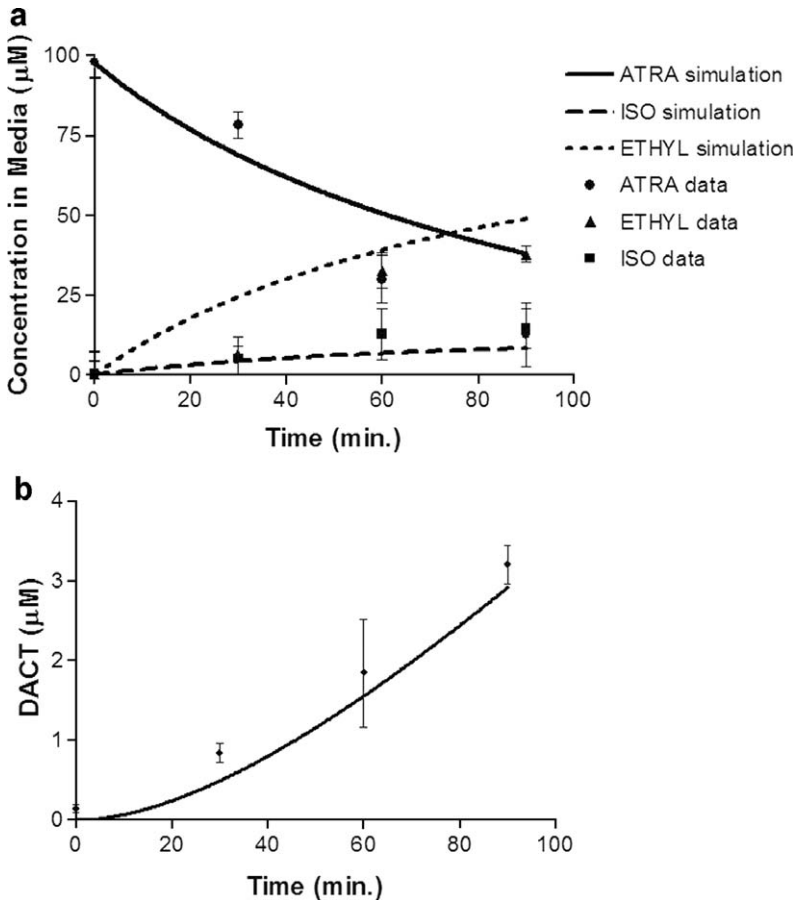

Fig. 5. Experimental data and competitive inhibition model simulations of (a) ATRA, ETHYL, ISO and (b) DACT after 98 μM ATRA treatment. Lines represent model simulations. Points represent data mean ± SD. The best fits were developed using Model III after sequential model building efforts to constrain the parameter space searched by the fitting algorithm.

was not detected in the microsomal study by Hanioka et al. (1999b). The lack of DACT production in this former study was likely due to the incubation conditions where high concentrations of ATRA (up to 200 μM) were incubated for short times, 20 min, rather than 90 min in our study. Consistent with these microsomal data, the present work indicated that DACT formation would be minimal at high incubation concentrations of ATRA due to inhibition of oxidative metabolism of ETHYL and ISO to DACT. A more accurate determination of the rates of oxidative metabolism of the mono-dealkylated metabolites to DACT requires kinetic studies in a hepatocyte incubation system using the mono-dealkylated metabolites as substrates.

Although the final model structure provided a good estimate to the majority of the data sets, the 1.7 μM DACT data were consistently underestimated. This discrepancy likely reflects analytical limitations at this lowest concentration where the sum of ATRA and all chlorinated products was frequently greater than the initial ATRA concentration. However, these data were most important for assessing the first-order clearance of ATRA from the incubation media and to determine the proportion of ETHYL and ISO produced by ATRA oxidation rather than providing final estimates of the kinetic constants for the downstream steps. These aspects were adequately simulated even though the measured DACT, near the limit of detection was considered less reliable.

In addition to oxidative metabolic clearance, ATRA and its chlorinated metabolites are also metabolized in the liver by glutathione conjugation to non-chlorinated metabolites. We did not attempt to measure GSH conjugates in this study and can make no statement of their presence after the 90 min incubations. Nonetheless, we did consider additional clearance from the incubation system due to GSH conjugation or production of other metabolites not monitored in this study. However, the mass balances for the time-course studies and the subsequent kinetic analysis indicated that this loss was small compared to the oxidative metabolic clearance.

4.2. Evaluation of competitive metabolic inhibition

These kinetic models provide useful tools to examine possible mechanisms such as metabolic interactions that might be responsible for the kinetic behaviors of compounds. An interesting outcome in this study was the observation that the greatest DACT production occurred

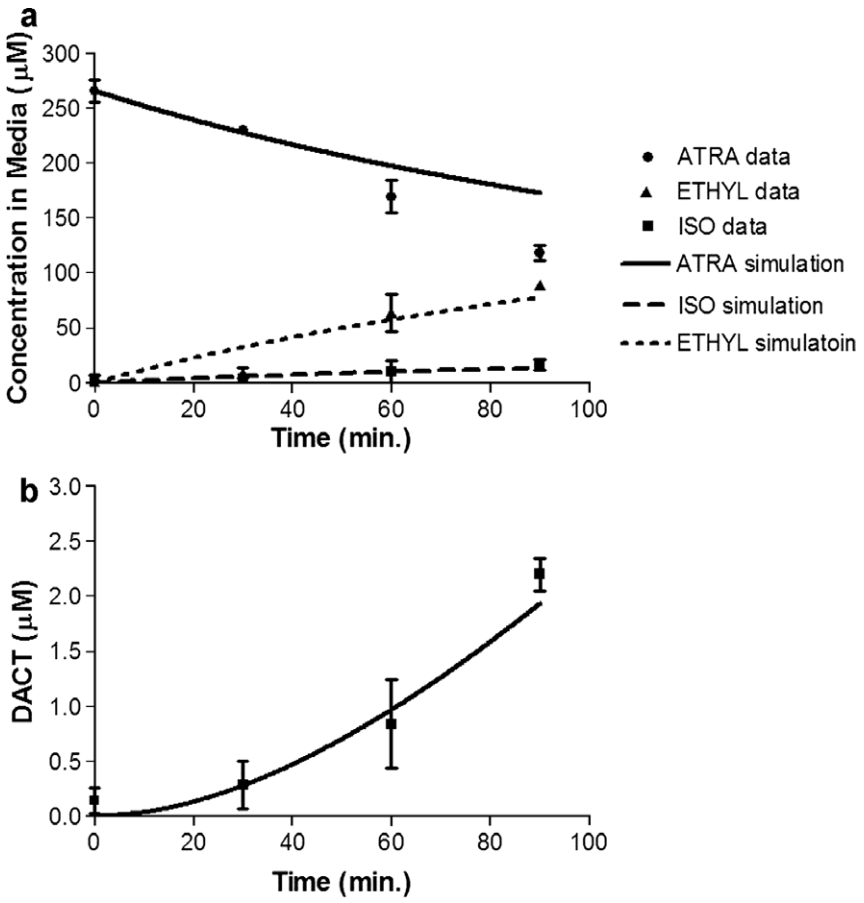

Fig. 6. Experimental data and competitive inhibition model simulations of (a) ATRA, ETHYL, ISO and (b) DACT after 266 μM ATRA treatment. Lines represent model simulations. Points represent data means ± SD. The best fits were developed using Model III after sequential model building efforts to constrain the parameter space searched by the fitting algorithm.

at 44 μM and subsequently decreased with increasing substrate concentration, indicating dose-dependent suppression of oxidative CYP family metabolism of mono-dealkylated metabolites at high ATRA concentrations, an observation consistent with inhibition of downstream oxidation by parent compound. We evaluated one mechanism of inhibition related to competitive inhibition by all Cl-TRIs. Inclusion of competitive metabolic inhibition by all Cl-TRIs was necessary to describe the non-linear characteristics of DACT while providing an internally consistent and biochemically realistic set of model parameters that could simultaneously simulate the other Cl-TRIs at all 4 concentrations. This competitive inhibition model (Model III) was successful in describing the time-courses of the Cl-TRIs across the 4 concentrations. Other more complex inhibition models might also work, but we used the most simple for this analysis.

Dose-dependent inhibition of product formation has been observed *in vitro* and *in vivo* with compounds in which both the parent compound and metabolite(s) are extensively metabolized by the same enzyme. For example, progressive oxidative metabolism of *n*-hexane to methyl-*n*-butyl ketone (MNBK) and MNBK to hexanedione (HD) causes dose-dependent formation of HD with maximum production at 1000 ppm that decreases with higher exposure concentrations (Baker and Rickert, 1981). This kinetic behavior could only be described in a PBPK model by competitive metabolic inhibition by hexane (Andersen and Clewell, 1983). In this model, MNBK production becomes saturated with increasing exposure and the conversion of MNBK to HD is inhibited as hexane concentrations increase. Similar to hexane kinetics, an *in vitro* model was developed to determine kinetic parameters for oxidative metabolism of benzene to phenol and the subsequent metabolism of phenol to hydroquinone and catechol from data obtained in mouse and rat microsomes (Medinsky et al., 1996). The kinetic disposition of each compound was simulated by describing metabolism with competitive inhibition of phenol to hydroquinone by increasing benzene concentrations. With both benzene and hexane the low concentration competitive inhibition likely arises through sequential metabolism of parent and mono-oxygenated metabolites via CYP 2E1. A similar interaction appears likely with ATRA and its metabolites.

In summary, this kinetic analysis evaluated the time-course behavior of oxidative metabolism of ATRA to the Cl-TRI metabolites using freshly isolated rat hepatocytes. The approach presented in this paper demonstrates the utility of kinetic modeling for examining mechanisms that regulate the time and dose-dependent kinetic disposition

of compounds (i.e., competitive metabolic inhibition). Although competitive metabolic inhibition occurs at high substrate concentrations within this *in vitro* system, this phenomenon still needs to be examined under *in vivo* situations to assess its relevance for toxicity testing or risk assessment. For instance, specific *in vivo* kinetic studies need to be done at different oral ATRA doses to see if there is a transient or more persistent decrease in DACT formation with increasing dose of ATRA. *In vitro* studies with mono-dealkylated Cl-TRI incubated with mass labeled ATRA could also provide direct data sets to analyze for various mechanisms of inhibition. Finally, the parameterization process developed to determine the *in vitro* kinetic constants for metabolism shows a useful strategy for curve fitting that accounts for the differential sensitivity of model parameters in the different concentration regimes used in the incubations. This procedure allowed analysis of the hypothesis that competitive interactions were occurring between metabolism of ATRA and its two monodealkylated metabolites.

Acknowledgements

Funding for this work was provided in part by the Syngenta Corporation Grant #53039.

References

Andersen, M.E., Clewell 3rd., H.J., 1983. Pharmacokinetic interactions of mixtures. In: Proceedings of the 14th Annual Conference on Environmental Toxicology, Dayton, Ohio, AFAMRL-TR-83-099, pp. 226–238.

Andersson, T.B., Sjoberg, H., Hoffmann, K.J., Boobis, A.R., Watts, P., Edwards, R.J., Lake, B.G., Price, R.J., Renwick, A.B., Gomez-Lechon, M.J., Castell, J.V., Ingelman-Sundberg, M., Hidestrand, M., Goldfarb, P.S., Lewis, D.F., Corcos, L., Guillouzo, A., Taavitsainen, P., Pelkonen, O., 2001. An assessment of human liver-derived in vitro systems to predict the in vivo metabolism and clearance of almokalant. Drug Metabolism and Disposition 29, 712–720.

Baker, T.S., Rickert, D.E., 1981. Dose-dependent uptake, distribution, and elimination of inhaled *n*-hexane in the Fischer-344 rat. Toxicology and Applied Pharmacology 61, 414–422.

Bakke, J.E., Larson, J.D., Price, C.E., 1972. Metabolism of atrazine and 2-hydroxyatrazine by the rat. Journal of Agricultural and Food Chemistry 20, 602–607.

Berry, M.N., Friend, D.S., 1969. High-yield preparation of isolated rat liver parenchymal cells: a biochemical and fine structural study. Journal of Cell Biology 43, 506–520.

Billings, R.E., McMahon, R.E., Ashmore, J., Wagle, S.R., 1997. The metabolism of drugs in isolated rat hepatocytes. A comparison with in vivo drug metabolism and drug metabolism in subcellular liver fractions. Drug Metabolism and Disposition 5, 518–526.

Brzezicki, J.M., Andersen, M.E., Cranmer, B.K., Tessari, J.D., 2003. Quantitative identification of atrazine and its chlorinated metabolites in plasma. Journal of Analytical Toxicology 27, 1–5.

Chenery, R.J., Keogh, J.P., Rath, L.C., McWilliams, P., 1991. In vitro-in vivo extrapolation of xenobiotic metabolism. Symposium: In Vitro Toxicology: Mechanisms and New Technology, pp. 135–143.

Cole, C.E., Tran, H.T., Schlosser, P.M., 2001. Physiologically based pharmacokinetic modeling of benzene metabolism in mice through extrapolation from in vitro to in vivo. Journal of Toxicology and Environmental Health, Part A 62, 439–465.

Cooper, R.L., Stoker, T.E., Tyrey, L., Goldman, J.M., McElroy, W.K., 2000. Atrazine disrupts the hypothalamic control of pituitary-ovarian function. Toxicological Sciences 53, 297–307.

Dauterman, W., Mueke, W., 1973. In vitro metabolism of atrazine by rat liver. Pesticide Biochemistry and Physiology 4, 212–219.

Eldridge, J.C., Minnema, D., Breckenridge, C.B., McFarland, J.E., Stevens, J.T., 2001. Effect of 6 months of atrazine or hydroxyatrazine on the leutinizing hormone surge in female Sprague–Dawley and Fischer 344 rats. The Toxicologist.

Gysin, H., Knuesli, E., 1960. Chemistry and herbicidal properties of triazine derivatives. In: Metcalf, R. (Ed.), Advances in Pest Control Research, vol. 3. Wiley (Interscience), New York, NY, pp. 289–358.

Hanioka, N., Jinno, H., Kitazawa, K., Tanaka-Kagawa, T., Nishimura, T., Ando, M., Ogawa, K., 1998. In vitro biotransformation of atrazine by rat liver microsomal cytochrome P450 enzymes. Chemico-Biological Interactions 116, 181–198.

Hanioka, N., Jinno, H., Tanaka-Kagawa, T., Nishimura, T., Ando, M., 1999a. In vitro metabolism of simazine, atrazine and propazine by hepatic cytochrome P450 enzymes of rat, mouse and guinea pig, and oestrogenic activity of chlorotriazines and their main metabolites. Xenobiotica 29, 1213–1226.

Hanioka, N., Jinno, H., Tanaka-Kagawa, T., Nishimura, T., Ando, M., 1999b. In vitro metabolism of chlorotriazines: chracterization of simazine, atrazine, and propazine metabolism using liver microsomes from rats treated with various cytochrome P450 inducers. Toxicology and Applied Pharmacology 156, 195–205.

Kedderis, G.L., Carfagna, M.A., Held, S.D., Batra, R., Murphy, J.E., Gargas, M.L., 1993. Kinetic analysis of furan biotransformation by F-344 rats in vivo and in vitro. Toxicology and Applied Pharmacology 123, 274–282.

Lang, D., Criegee, D., Grothusen, A., Saalfranck, R.W., Bocker, R.H., 1996. In vitro metabolism of atrazine, terbuthylazine, ametryne, and terbutryne in rats, pigs, and humans. Drug Metabolism and Disposition 24, 859–865.

McMullin, T.S., Brzezicki, J.M., Cranmer, B.K., Tessari, J.D., Andersen, M.E., 2003. Pharmacokinetic modeling of disposition and time-course studies with [^{14}C]atrazine. Journal of Toxicology and Environmental Health, Part A 66, 941–964.

McMullin, T.S., Andersen, M.E., Nagahara, A., Lund, T.D., Pak, T., Handa, R.J., Hanneman, W.H., 2004. Evidence that atrazine and diaminochlorotriazine inhibit the estrogen/progesterone induced surge of LH in female Sprague–Dawley rats without changing estrogen receptor action. Toxicological Sciences 79, 278–286.

Medinsky, M.A., Kenyon, E.M., Seaton, M.J., Schlosser, P.M., 1996. Mechanistic considerations in benzene physiological model development. Environmental Health Perspectives 104 (Suppl. 6), 1399–1404.

Nakajima, T., Wang, R.S., Murayama, N., Sata, A., 1990. Three forms of trichloroethylene-metabolizing enzymes in rat liver induced by ethanol, phenobarbital, and 3-methylcholanthrene. Toxicology and Applied Pharmacology 102, 546–552.

Seglen, P.O., 1976. Preparation of isolated rat liver cells. Methods in Cell Biology 13, 29–83.

Sirica, A.E., Pitot, H.C., 1979. Drug metabolism and effects of carcinogens in cultured hepatic cells. Pharmacological Reviews 31, 205–228.

Thede, B., 1987. Study of ^{14}C-Atrazine Dose/Response Relationship in the Rat. Ciba-Geigy Corporation, Greensboro, North Carolina, pp. 1–33.

Thede, B., 1988. Comparative Metabolism of Atrazine by Mammalian Hepatocytes: Progress Report. Ciba-Geigy Corporation, Greensboro, North Carolina.

Thurman, R.G., Kauffman, F.C., 1979. Factors regulating drug metabolism in intact hepatocytes. Pharmacological Reviews 31, 229–251.